Measurement of resonant x-ray magnetic scattering from induced Cu polarizations in exchange-coupled Co/Cu multilayers

2004 J. Phys.: Condens. Matter 16 1915

(http://iopscience.iop.org/0953-8984/16/12/002)

INSTITUTE OF PHYSICS PUBLISHING JOURNAL OF PHYSICS: CONDENSED MATTER

J. Phys.: Condens. Matter **16** (2004) 1915–1925 PII: S0953-8984(04)74541-5

Measurement of resonant x-ray magnetic scattering from induced Cu polarizations in exchange-coupled Co/Cu multilayers

Y Hayasaki[1], K Ishiji[1], H Hashizume[1,4], N Hosoito[1], K Omote[2], M Kuribayashi[2], G Srajer[3], J C Lang[3] and D Haskel[3]

[1] Research and Education Centre for Materials Science, Nara Institute of Science and Technology, Ikoma, Nara 630-0192, Japan
[2] Rigaku Corporation, Akishima, Tokyo 196-8666, Japan
[3] Advanced Photon Source, Argonne National Laboratory, Argonne, IL 60439, USA

E-mail: hhashizu@ms.aist-nara.ac.jp

Received 9 January 2004
Published 12 March 2004
Online at stacks.iop.org/JPhysCM/16/1915 (DOI: 10.1088/0953-8984/16/12/002)

Abstract

An avalanche photodiode detector has been commissioned to measure weak resonant x-ray magnetic scattering (RXMS) from induced magnetic polarizations in Cu layers in exchange-coupled Co/Cu multilayers using circularly polarized x-rays from synchrotron sources. The detector can count x-rays at rates of 10^7 photons s^{-1}, giving good estimates of the RXMS at superlattice Bragg peaks in a reasonably short time when count losses due to the time structure of the synchrotron x-rays are corrected for. RXMS superlattice Bragg peaks as small as 1×10^{-4} in flipping ratio have been measured from a Co/Cu multilayer at the K absorption edge of Cu. The data are fitted by an oscillatory model magnetization profile in the Cu layers derived from a Ruderman–Kittel–Kasuya–Yosida theory of exchange coupling adapted to a planar geometry.

1. Introduction

Resonant x-ray magnetic scattering (RXMS) is a powerful probe to explore the partial magnetic structures of compound materials, alloys and nanostructures [1]. RXMS has the element and electron-shell specificity the same as x-ray magnetic circular dichroism (XMCD). This useful property originates in the significant enhancement of magnetic scattering from resonating atoms near the absorption edges. RXMS, also called exchange scattering [2], is resonant magnetic-charge interference scattering [3], which is much stronger than pure magnetic scattering from off-tuned atoms. This enables the structures formed by weak magnetic

[4] Address for correspondence: 8916-5 Takayama, Ikoma 630-0192, Japan.

moments induced on 'nonmagnetic' atoms to be probed in the presence of nearby ferromagnetic atoms [1, 4]. With neutrons, one can distinguish magnetic scattering from one species of atom from another only for well-ordered periodic structures. To isolate RXMS from the overwhelming charge scattering, one can illuminate a sample with a linearly polarized x-ray beam and analyse the polarization of scattered x-rays [2]. Alternatively, one uses circularly polarized x-rays of alternating helicities and calculates the difference $I^+ - I^-$, where I^+ and I^- are the scattering intensities observed for the + and − helicities of primary x-rays, respectively [1, 4, 5]. The latter technique is preferred in the investigation of multilayered samples because the polarization factor $\cos 2\theta$ retains a large value at small scattering angles 2θ [1]. In contrast, the $\sin 2\theta$ polarization factor for linearly polarized primary x-rays reduces the magnetic scattering intensity at small 2θ. Magnetic polarizations of 'nonmagnetic' metals play a central role in thin-film magnetism like indirect exchange couplings, giant magnetoresistance and spin valves [6].

At third-generation synchrotron sources, I^+ and I^- from metal multilayers are highly intense, often exceeding 10^8 cps, which cannot be coped with by conventional NaI(Tl) scintillator/photomultiplier combinations but is too weak to be measured using analogue detectors like ion chambers. One can reduce the count rate by placing attenuator plates in the beam path or by narrowing down the slit aperture, but this leads to a prolonged count time to achieve reasonable statistics in $I^+ - I^-$ at each 2θ. The weakest measurable RXMS is practically limited by the high count-rate capability of a detector. Our experience shows that, with a standard NaI counter of 1 μs dead time, this limit is located not far from 1×10^{-3} in flipping (or asymmetry) ratio $(I^+ - I^-)/(I^+ + I^-)$. This is just enough to measure the RXMS from ferromagnetic 3d transition metals at the K absorption edges [1] and the paramagnetic states of rare earths at the L edges [4]. A faster x-ray detector is required to probe the weaker magnetism of 'nonmagnetic' metals.

In this paper, we will show that avalanche photodiode (APD) detectors fit this purpose. We present the design and general performance of a silicon APD detector in section 2 and investigate, in section 3, its behaviour in measuring RXMS at count rates as high as 10^7 photons s^{-1} using circularly polarized x-rays from a synchrotron source. Section 4 is dedicated to a measurement of RXMS superlattice Bragg peaks from an exchange-coupled Co/Cu multilayer at the K adsorption edge of Cu. We will present a model magnetization profile in the Cu layers that fits the RXMS data and discuss its significance in the indirect exchange coupling. Finally, section 5 concludes the paper.

2. APD detector and experimental set-up

The work described here has been done with a photodiode made by Hamamatsu Photonics. The nominal area available for x-ray detection is 3 mm × 5 mm. The diode has a silicon $p^+/\pi/p/n$ structure, mounted on a ceramic disc 13.9 mm in diameter with the n surface upwards. The π layer is charge depleted when the diode is reversely biased. We masked the diode with a 15 μm-thick aluminium foil to shut out visible light. The same APD is available on a G10 glass-epoxy back plate with a 3 mm × 5 mm through-hole bored. This type allows x-rays to impinge on the p^+ surface, which provides a higher energy resolution of ∼20% at 16.5 keV [7, 8]. The active thickness of the detector is defined by the thickness of the depletion layer, which is ∼130 μm in our APD for 440 V reverse bias applied. This provides a detection efficiency of 74% for x-rays of the energy of the Cu K absorption edge. According to the maker's data sheet, the electron multiplication factor (gain) in the APD is ∼100 at this bias voltage with a dark current of 20 nA at room temperature. As in semiconductor detectors, the rise time of the output signal pulses depends on the charge collection time in the diode, the diode capacitance and the

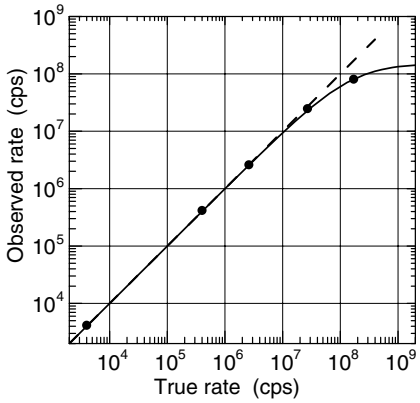

Figure 1. Linearity response of the APD detector. The true rates were estimated by attenuating the probing x-ray beam at a classical source.

time constant of the associated amplifier. While amplifiers for semiconductor detectors are designed for low noise and high gain, the primary concerns in amplifiers for APDs are a wide bandwidth and a moderate gain. Using a homemade amplifier, which is 1 GHz in bandwidth and 200 in gain, we observed signal pulses of ∼2 ns in FWHM. The mean pulse height for 8 keV input x-rays is ∼20 mV with a noise level of 2–4 mV. Setting a discriminator at 10 mV shows a dark count rate of less than 0.1 cps. Figure 1 shows a linearity response of the detector system using a SRS (Stanford Research Systems) model SR400 photon counter as a scaler. In practice, the system is linear up to 1×10^7 cps. Full circles show the rates observed at a classical x-ray generator, which are fitted by the full line, calculated for a nonparalyzeable Poissonian detector [9] with a 7 ns dead time[5]. With dead-time corrections applied, the system allows us to handle rates of 10^7 cps.

A good way to minimize various instabilities in an experimental set-up for RXMS using circularly polarized hard x-rays is to periodically flip the helicity by rotary oscillating a quarter-wavelength phase plate [10] and to synchronously measure I^+ and I^- [1, 5]. This is preferred to a sequential measurement. A diamond phase retarder works well for 5–15 keV x-rays, which provides a high degree of circular polarization exceeding 90%, as well as a high transmission efficiency. Figure 2 shows a set-up used on beamline BL39XU at SPring-8, Japan Synchrotron Radiation Research Institute. We converted the linearly polarized x-rays from the undulator source into circularly polarized light using a 0.45 mm-thick (111) diamond crystal in the $2\bar{2}0$ Laue-diffraction geometry. A piezoelectric driver rotary oscillated the crystal back and forth across the $2\bar{2}0$ position in accordance with a train of square signals of 50% duty cycle (frequency f) obtained from a function generator. The same signal is used to gate a dual-channel photon counter SR400. In channel 1 is fed the APD output, whereas channel 2 measures the ion-chamber current via a 1 MHz voltage/frequency converter. The latter serves as an x-ray intensity monitor. In the timing diagram of figure 3, gate delay is an allowance to wait to begin counting in the SR400 until the phase plate stabilizes at a predetermined angular position after a rotation. The count time in SR400 is defined by gate open. Typically, we use 10 and 390 ms for gate delay and gate open, respectively, for $f = 1$ Hz. Figures 2 and 3 may remind readers of the set-up described in [11]. A remark will be made on this point in a later section of this paper.

[5] This is slightly larger than the 5 ns pulse-pair resolution specified for SR400.

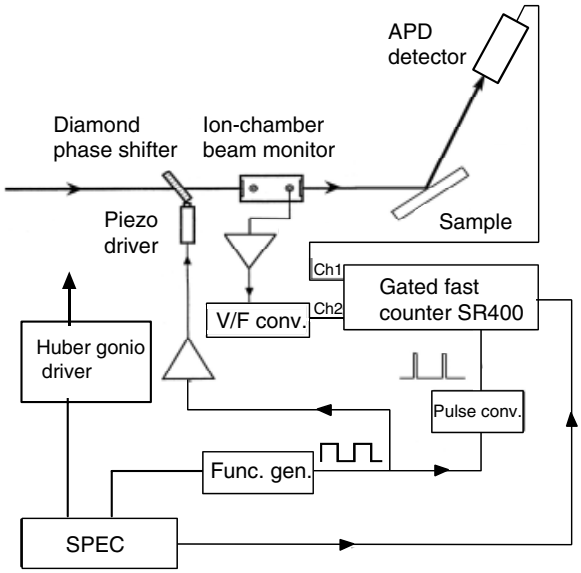

Figure 2. Set-up for RXMS measurements using circularly polarized probing x-rays with the APD detector at the 4-ID-D station of the Advanced Photon Source. SPEC indicates a UNIX programme controlling the measurements. At SPring-8 LabView is used in place of SPEC.

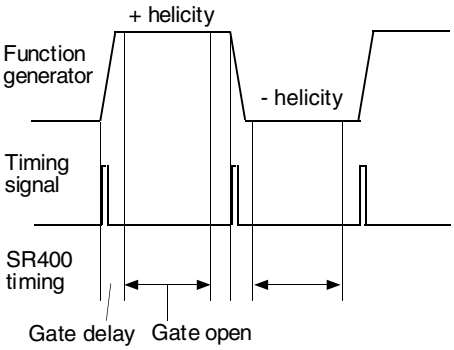

Figure 3. Timing diagram for helicity modulation measurements of RXMS. See the text for gate delay and gate open.

3. Measurement of resonant magnetic scattering

We investigated the count-rate behaviour of our detector system by measuring the first-order superlattice Bragg peak from a multilayered Cu(1.9)/[Co(1.2)/Cu(1.9)]$_{50}$/Ta(5.0 nm)/Si-sub sample near the K absorption edge of Co. A strong enough in-plane field was applied on the sample to align the magnetization vectors along the direction either parallel or antiparallel to the projection of the x-ray wavevector onto the sample plane. +1000 and −1000 Oe indicate such parallel and antiparallel fields, respectively. We maximized the difference scattering intensity $I^+ - I^-$ by tuning the x-ray energy to 7720 eV, at which the real part of the resonant magnetic scattering factor for Co was maximal. With a beam size of 0.1(V) × 0.5(H) mm, the peak count rate observed on the first Bragg peak was 3.1×10^7 cps, which we attenuated to the desired

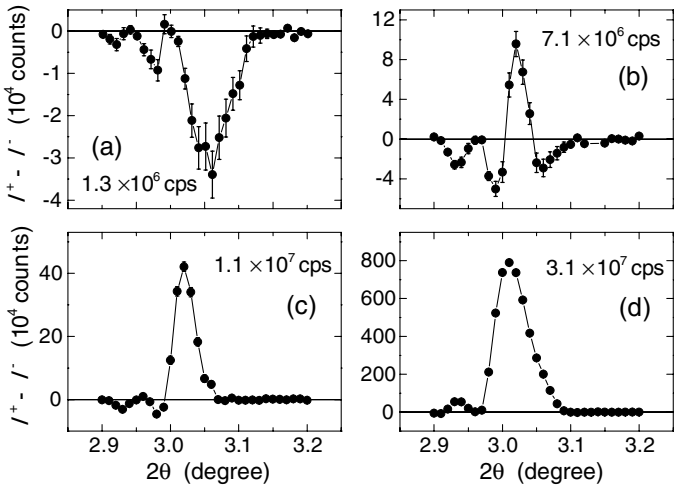

Figure 4. Difference profiles of the first-order Bragg peak observed from the Co(1.2)/Cu(1.9 nm) multilayer sample at the Co K edge at count rates of 1.3×10^6 cps (a), 7.1×10^6 cps (b), 1.1×10^7 cps (c) and 3.1×10^7 cps (d) on the APD detector. An in-plane field of +1000 Oe was applied to the sample. The count time per point is 11.7 s for I^+ and I^-. The I^+ and I^- data are scaled to the monitor ion-chamber outputs. Error bars show photon statistics.

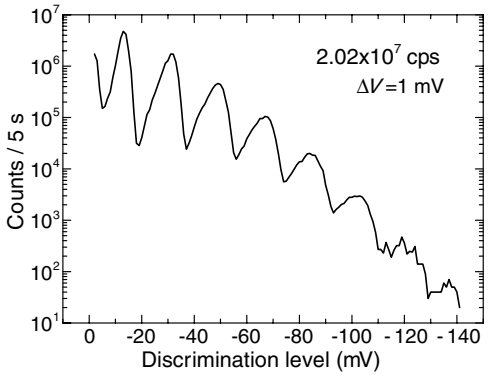

Figure 5. Pulse-height spectrum observed for 7720 eV x-rays at 2.02×10^7 cps. The discriminator window ΔV is set at 1 mV. Single events are seen at -13 mV, accompanied by 2–8 multiple events at higher pulse heights. Note that the amplifier is inverting. The data were obtained by fanning out the APD output to channels 1 and 2 of the SR400 with their discriminators set at L and $L + 1$ mV and scanning L.

rates with the use of aluminium foils. Figure 4 shows the difference peak profiles observed at the peak count rates indicated in the individual panels. In these and all other measurements, except the one shown in figure 5, we set the built-in discriminator of SR400 at 10 mV. It is striking to see in figure 4 that the $I^+ - I^-$ profiles systematically vary from a negative peak at 'low six' (1.3×10^6 cps) to a positive peak at 'medium low seven' (3.1×10^7 cps). This behaviour is related to the time structure of synchrotron x-rays.

The SPring-8 light source was filled with $203 - 7 \times 4$ electron bunches at the time of the experiment (8 GeV, 100 mA). The 1436 m long orbit was uniformly populated by 203 bunches, of which 4 successive bunches were missing in 7 locations. Each time an electron bunch passes

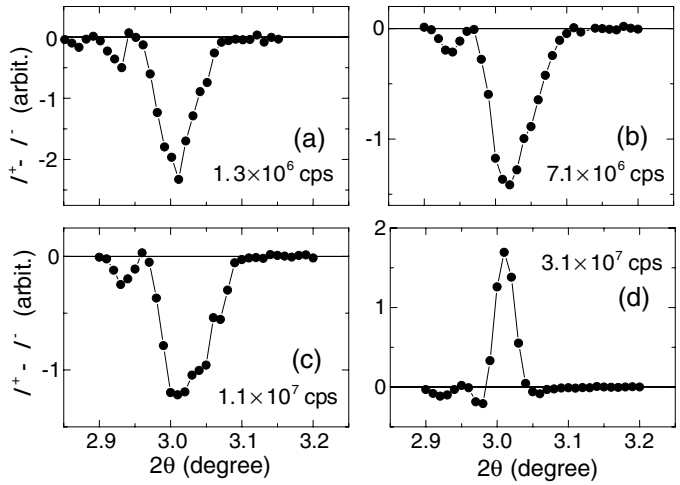

Figure 6. Difference peak profiles corrected for the count losses using equation (1).

through the tangent point of a beamline, an x-ray flash of 31.8 ps time duration (FWHM) is delivered. X-ray flashes thus arrive at the APD detector at a shortest time period of 23.6 ns (T_b) in this fill mode. Our detector system, having the dead time of 7 ns (τ_d), resolves individual x-ray flashes but may count only one at most per flash. n detected photons in a flash produce a piled-up pulse of n times larger amplitude. This is shown in the pulse height spectrum of figure 5, where single events are seen at -13 mV, followed by 7 successive multiple events. For a n multiple event, the detector system counts one and $n-1$ counts are lost. The highest possible count rate in the SR400 should thus equal the mean bunch rate (36.6 MHz). Let the average number of photons impinging on the APD per flash be q and assume the Poisson statistics for incoming photons in a flash. The number q' of detected photons is then given by

$$q' = 1 - e^{-q}. \tag{1}$$

q' equals 0.55 at a count rate of 2×10^7 cps, for which equation (1) gives $q = 0.8$. At the limit rate of 36.6×10^6 cps, we have $q' = 1$ and $q = \infty$. Note that equation (1) does not involve the detector's dead time τ_d nor the detection efficiency η, which is 77% for 7720 eV x-rays including absorption by the aluminium input window. This may appear to be strange, but is justified for $t_f < \tau_d < T_b$, where t_f stands for the time width of an x-ray flash.

Applying equation (1) to the data of figure 4 produces drastic changes in the peak profiles. Those for 'high six' and 'low seven' now show negative peaks (figures 6(b) and (c)), which are akin to the one for 'low six' (figure 6(a)). The observed peak count rate for figure 6(d) is 3.1×10^7 cps, which is close to the limit rate of 3.66×10^7 cps. Even though equation (1) is valid at this high rate, a small error in the observed count rate (q') results in a large error in the corrected rate (q). We understand that this explains why the corrected peak profile in figure 6(d) looks similar to the raw one in figure 4(d). It is a usual procedure in RXMS experiments to repeat a measurement of $I^+ - I^-$ after applying a reversed magnetic field on the sample and to calculate the difference between two $I^+ - I^-$ results to eliminate offsets including nonmagnetic dichroic effects. In figure 7 full and open symbols show the flipping ratios $(I^+ - I^-)/(I^+ + I^-)_{BP}$ of the RXMS observed before (+1000 Oe) and after (-1000 Oe) the field reversal, respectively. The two profiles in each of figures 7(a)–(c), for the observed peak count rates lower than 'low seven', show opposite polarities even though they are not quite symmetrical. Figure 8 compares the peak profiles in $(F(+) - F(-))/2$ for the four count

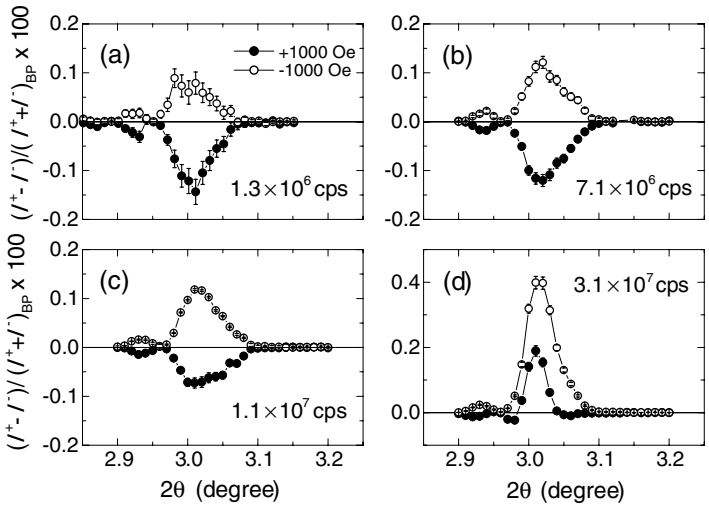

Figure 7. Flipping ratios observed for the first-order Bragg peak from the Co/Cu multilayer sample at the Co K edge at count rates of 1.3×10^6 cps (a), 7.1×10^6 cps (b), 1.1×10^7 cps (c) and 3.1×10^7 cps (d) on the APD detector. External in-plane fields of +1000 Oe and −1000 Oe were applied on the sample. The data shown by the full symbols are the same as those in figure 6. Error bars indicate photon statistics.

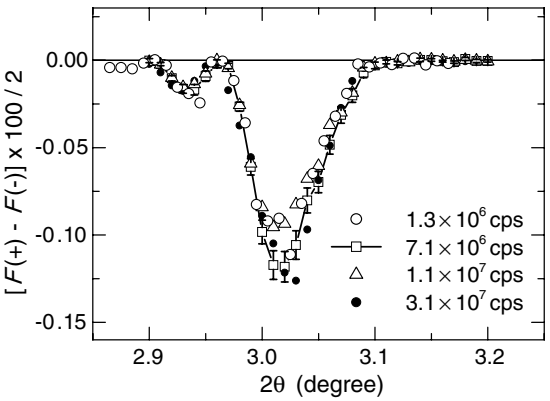

Figure 8. Flipping ratios averaged over the reversed-field measurements for the peak count rates indicated. The data are the same as those shown in figure 7. Error bars show photon statistics for the measurement at 7.1×10^6 cps.

rates tested, where $F(+)$ is the flipping ratio $(I^+ - I^-)/(I^+ + I^-)_{\mathrm{BP}}$ for the + field. The three profiles for 'low six', 'high six' and 'low seven' show a fair agreement within the error bars. Surprisingly, the data for the 'medium low seven' (3.1×10^7 cps) reside very close. In the limit of the very high count rates, the APD should saturate at the bunch rates of 3.66×10^7 cps and the difference $I^+ - I^-$ should vanish. It is highly likely that our APD detector correctly measures RXMS of 0.1% in flipping ratio at observed count rates up to 'low seven' in I^+ and I^-, but we should be careful with the fill mode of synchrotron sources. At a source filled with many more electron bunches than the present one, one would count at rates of 'medium seven', still giving a good estimate of RXMS.

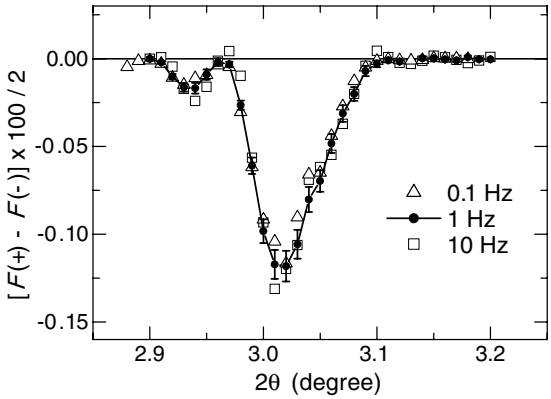

Figure 9. First-order Bragg peak from the same sample as in figure 8, observed by switching the photon helicity at 0.1, 1 and 10 Hz. The peak count rates are at 'high six'. Error bars show photon statistics for the measurement with 1 Hz.

Periodic oscillation of the x-ray phase plate and synchronous collection of the I^+ and I^- data is primarily to avoid adverse effects of long-term drifts. It may serve as well to improve the signal-to-noise ratio of the data. To see if this is true, we changed the frequency f of the oscillation to 0.1 and 10 Hz and repeated the measurement described in figure 7. The count time per point was nearly fixed at 10 s in I^+ and I^-. We controlled the peak count rates at 'high six' (ranging from 6.6×10^6 to 7.6×10^6 cps). The result in figure 9 shows that there is no practical difference between the qualities of the three sets of data. Nevertheless, it demonstrates an excellent reproducibility, and hence a high reliability, of the measurement. One would profit from this mode of data collection when measuring RXMS from extremely weak magnetic polarizations over an extended time. An optimum frequency f will depend on specific set-ups, which has to be sorted out. We may call this mode a digital lock-in mode, though it is not phase-sensitive as in [11].

4. Measurement of RXMS from Cu polarizations

We applied our APD detector to a measurement of RXMS from magnetizations induced on Cu. The sample employed is a Co/Cu multilayer of a slightly different design, $[\mathrm{Co}(1.25)/\mathrm{Cu}(3.88\ \mathrm{nm})]_{50}$ on a silicon substrate, grown by magnetron sputter deposition in a high-vacuum chamber. We tuned the primary x-ray energy to 8991 eV, close to the K edge of Cu, on the 4-ID-D beamline at the Advanced Photon Source (APS)[6], Argonne National Laboratory, and applied fields to magnetically saturate the sample in plane (+540 and −540 Oe in this case). Figure 10(a) shows the averaged flipping ratios, $(F(+) - F(-))/2$, observed at the first-, second- and third-order superlattice Bragg peak positions. Note that the RXMS smaller than 4×10^{-4} indicates a very weak magnetic polarization induced on the 4p states of Cu electrons. We modestly limited the peak count rates on the APD to $\sim 3 \times 10^6$ cps with the use of attenuator plates. The raw $I^+ - I^-$ data include $\sim 1 \times 10^5$ photon counts at the top of the first peak, located at $2\theta = 1.7^\circ$ in figure 10(a), which were measured in 60 s. The total scan time for the three peaks in figure 10(a) is 400 min. Noting that the bunch rate at APS was 90 MHz, we could have counted at a 'low seven' to acquire data of a similar quality in a few hours.

[6] The energy calibration on 4-ID-D was discovered to be shifted by +2 eV from the one at BL39XU.

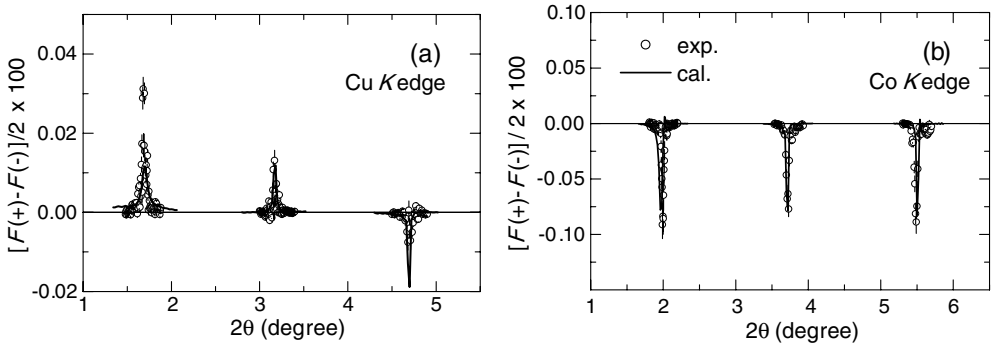

Figure 10. RXMS superlattice Bragg peaks observed from a $[\mathrm{Co}(1.25)/\mathrm{Cu}(3.88\ \mathrm{nm})]_{50}$ multilayer at the Cu K edge (a) and the Co K edge (b). The count time per point is 110 s for (a) and 28 s for (b). The raw $I^+ - I^-$ data include $\sim 1 \times 10^5$ photon counts at the top of the first peak at $2\theta = 1.7°$ in (a), which were measured in 60 s. Error bars show photon statistics. Note the distinct vertical scales in (a) and (b). For the full line see text.

The three peaks in figure 10(a) show positive or negative profiles, depending on the reflection order. This indicates that the 4p states of Cu sandwiched between the Co layers are nonuniformly spin polarized along the out-of-plane direction. In contrast, all three Bragg peaks show the same polarity in figure 10(b), observed from the same sample at the Co K-edge. This is a plausible observation since the 4p states in the ferromagnetic Co layers are expected to be spin polarized to a same extent everywhere. Indeed, the data are well fitted by a model assuming uniformly magnetized Co layers (full line in figure 10(b)). The total scan time for the three peaks in figure 10(b) is 100 min. Clearly, the APD detector is a significant improvement over the existing detectors even when measuring RXMS of 0.1%. It is worth noting that the flipping ratio of the RXMS observed from the multilayered Co/Cu at the Cu K edge is of the same order of magnitude as the XMCD signals reported in [12]. This agreement is by no means accidental since RXMS and XMCD are fundamentally linked through the optical theorem [3]. It ensures that figure 10(a) presents an essentially correct estimate of the RXMS from Cu in the multilayered Co/Cu.

While the XMCD defined by $\Delta\mu/\mu_{\mathrm{jump}}$ represents an average magnetization over the sample thickness, momentum-resolved RXMS as a function of 2θ provides information on the spatial distribution of magnetic polarizations of the tuned states in the direction of the scattering vector $\boldsymbol{q}$. The full line in figure 10(a) shows a fit to the data, which is calculated from the model polarization profile of figure 11 for the 4p electrons in the Cu layer. In the RKKY (Rutherman–Kittel–Kasuya–Yosida) picture, an oscillatory magnetic polarization, $P(z)$, is induced on nearly free electrons in the Cu layer through magnetic interactions with the ferromagnetic Co layer at the interface [13–15]. In our Co/Cu multilayer placed in a strong external in-plane field, the Co moments are aligned parallel and the magnetic polarization in a Cu layer is a superposition of two polarization patterns emanating from each Co/Cu interface, $P(z) + P(t_{\mathrm{Cu}} - z)$, where t_{Cu} is the thickness of the Cu layer, which equals 3.88 nm in our sample. The functional form of $P(z)$ given in [16] shows a polarization diverging at the interface ($z = 0$), which is cut-off at $z = 0.244$ nm and replaced by P (0.244 nm) in figure 11. This profile is featured by the positive interface polarizations accompanied by the comparably large negative polarizations inside. This is essential to reproduce the Bragg peak signs observed in figure 10. Attempts to provide a better fit by refining the polarization profile in the vicinity of the interface will be reported elsewhere. A fit to the charge scattering data

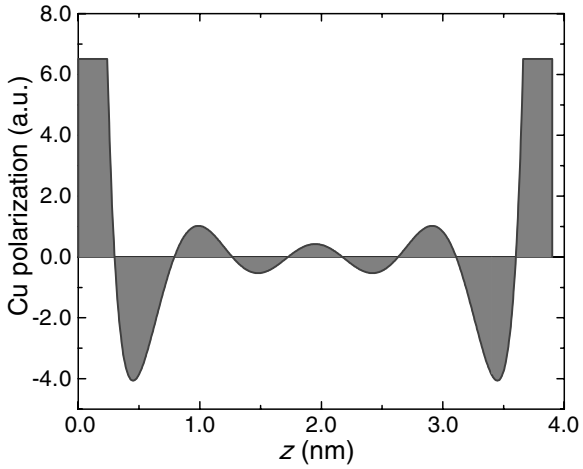

Figure 11. Magnetic polarization profile induced in the 3.88 nm-thick Cu layers used to calculate the full line in figure 10(a). A Cu layer is sandwiched between ferromagnetic Co layers with their interfaces located at $z = 0$ and 3.88 nm. The full line in figure 10(a) assumes this polarization pattern for the 50 Cu layers in the sample.

reveals smooth Co/Cu interfaces (0.37 nm in the root-mean-square roughness value) in our sample, as well as small dispersions of 0.01 nm in the thicknesses of the Co and Cu layers. The oscillatory polarization $P(z)$ propagates across the Cu layer and interacts with another Co layer, thereby giving rise to the magnetic coupling between the two Co layers. In fact, the Co/Cu multilayer studied here shows a giant magnetoresistance of 7% in $\Delta R/R$ on the third peak of the coupling oscillation [17]. Using the APD detector, one can now perform structural studies on indirect exchange couplings and nanomagnetic materials by RXMS measurements.

5. Concluding remarks

We have shown that the APD detector can probe magnetic structures of 'nonmagnetic' metal spacers sandwiched between ferromagnetic layers by allowing the RXMS to be measured in a reasonably short time at synchrotron sources. A weakest RXMS of 1×10^{-4} in flipping ratio was measured in this paper. Count-loss corrections are vital to estimate the RXMS from the measured scattering intensities at observed count rates greater than the low 10^6 cps. Appropriate corrections can be done by noting the time structure of synchrotron x-rays. We have observed the RXMS superlattice Bragg peaks from the weak magnetic polarizations induced on the Cu 4p electrons in an exchange-coupled Co/Cu multilayer and presented, for the first time, a model Cu polarization profile across the layer showing an oscillatory behaviour in accordance with the prediction by RKKY theory adapted to a planar geometry.

Acknowledgments

We thank T Ohkochi and T Murano for their help in data collection and R Kokufu for assistance in simulation calculation. The experiment at SPring-8 was supported under proposals nos. 2002B0462 and 2003A0480 and the one at APS under proposal no. GUP-100. The work at the Advanced Photon Source is supported by the US DOE, Office of Science, under contract no. W-31-109-ENG-38. This work is supported by Collaborative Research Projects of the Materials and Structures Laboratory, Tokyo Institute of Technology.

References

[1] Ishimatsu N, Hashizume H, Hamada S, Hosoito N, Nelson C S, Venkataraman C T, Srajer G and Lang J C 1999 *Phys. Rev.* B **60** 9596

[2] Gibbs D, Harshman D R, Issac E D, McWhan D B, Mills D and Vettier C 1988 *Phys. Rev. Lett.* **61** 1241
Hannon J P, Grammel G T, Blume M and Gibbs D 1988 *Phys. Rev. Lett.* **61** 1245

[3] Lovesey S W and Collins S P 1996 *X-ray Scattering and Absorption by Magnetic Materials* (Oxford: Oxford Science Press)

[4] Sève L, Jaouen N, Tonnerre J M, Raoux D, Bartolomé F, Arend M, Felsch W, Rogalev A, Goulon J, Gautier C and Bérar J F 1999 *Phys. Rev.* B **60** 9662
Jaouen N, Tonnerre J M, Raoux D, Bontempi E, Ortega L, Müezenberg M, Felsch W, Rogalev A, Dürr H A, Dudzik E, van der Laan E, Maruyama H and Suzuki M 2002 *Phys. Rev.* B **66** 134420

[5] Hashizume H, Ishimatsu N, Sakata O, Iizuka T, Hosoito N, Namikawa K, Iwazumi T, Srajer G, Venkataraman C T, Lang J C, Nelson C S and Berman L E 1998 *Physica* B **248** 133

[6] Himpsel F J, Ortega J E, Mankey G J and Willis R F 1998 *Adv. Phys.* **47** 511

[7] Baron A Q R, Rüffer R and Metge J 1997 *Nucl. Instrum. Methods Phys. Res.* A **400** 124

[8] Kishimoto S, Ishizawa N and Vaalsta T P 1998 *Rev. Sci. Instrum.* **69** 384

[9] Knoll G F 1989 *Radiation Detection and Measurement* (New York: Wiley)

[10] Hirano K, Ishikawa T, Koreeda S, Fuchigami K, Kanzaki K and Kikuta S 1992 *Japan. J. Appl. Phys.* **31** L1209
Giles C, Malgrange C, Goulon J, de Bergevin F, Vettier C, Fontaine A, Dartyge E and Pizzini S 1994 *Nucl. Instrum. Methods* A **349** 622

[11] Suzuki M, Kawamura N, Mizumaki M, Urata A, Maruyama H, Goto S and Ishikawa T 1998 *Japan. J. Appl. Phys.* **37** L1488
Suzuki M, Kawamura N and Ishikawa T 2001 *Proc. SPIE* **4145** 140

[12] Pizzini S, Fontaine A, Giorgetti C, Dartyge E, Bobo J-F, Piecuch M and Baudelet F 1995 *Phys. Rev. Lett.* **74** 1470

[13] Yafet Y, Kwo J, Hong M, Majkrzak C F and O'Brien T 1988 *J. Appl. Phys.* **63** 3453

[14] Bruno P and Chappert C 1991 *Phys. Rev. Lett.* **67** 1602
Bruno P and Chappert C 1992 *Phys. Rev.* B **46** 261

[15] Bruno P 1999 *J. Phys.: Condens. Matter* **11** 9403

[16] Ishiji K, Hashizume H and Hosoito N 2004 at press

[17] Parkin S S P, Bhadra R and Roche K P 1991 *Phys. Rev. Lett.* **66** 2152